JOURNAL OF GEOPHYSICAL RESEARCH, VOL. 103, NO. C5, PAGES 10,241–10,251, MAY 15, 1998

# Simulation of the South Atlantic Ocean circulation and its seasonal variability

Jianping Gan,[1] Lawrence A. Mysak, and David N. Straub

Department of Atmospheric and Oceanic Sciences, McGill University, Montreal, Quebec, Canada

**Abstract.** The high-resolution Princeton Ocean Model is used to simulate the circulation and seasonal variability of the South Atlantic Ocean. A diagnostic calculation, using the Levitus annual mean fields and forcing consisting of the climatological annual mean wind stress, produces a realistic steady circulation pattern. In particular, the meridional overturning cell shows equatorward flow in the surface and intermediate waters and poleward flow at depth. Associated with this circulation is a northward heat transport that reaches a maximum of 1 PW near 20°S. The model results are improved when the density field near the ocean bottom is allowed to deviate from the Levitus values. Using forcing consisting of observed monthly wind stress, heat flux and a prescribed seasonally varying Antarctic Circumpolar Current (ACC), a prognostic calculation is next carried out to study the seasonal variability in the South Atlantic Ocean. With a realistic heat flux, the model output for the seasonal thermal field compares well with that in the Levitus data. An analysis suggests that the seasonal cycle of the Brazil Current separation latitude, as well as the strength of the Falkland-Malvinas Current depends more strongly on the prescribed seasonal variability in the strength of the ACC than on the seasonal variations in wind and buoyancy forcing in the South Atlantic.

## 1. Introduction

The South Atlantic Ocean is the major conduit for water mass exchange between the North Atlantic Ocean, the Weddell Sea, and the Antarctic Circumpolar Current (ACC). Many previous studies of the South Atlantic circulation were based on water mass analyses of hydrographic data [e.g., *Reid*, 1977, 1989] and on the satellite IR images [e.g., *Matano et. al*, 1993]. The inferred upper level circulation in the South Atlantic is reviewed by *Peterson and Stramma* [1991]. As the main stream of the ACC moves eastward through Drake Passage, part of it branches northward near the Argentina shelf break and forms the Falkland-Malvinas Current (called FMC hereafter). The Brazil Current (BC), the western boundary current of the South Atlantic subtropical gyre, flows south along the eastern continental margin of South America. This warm, saline BC then meets the cold, fresh FMC near 40°S, the confluence zone where both currents separate from the coast. Part of the BC continuously flows southward and can reach as far as 46°S [*Legeckis and Gordon*, 1982]. At midlatitudes in the eastern South Atlantic, the subtropical gyre is closed by an eastern northward flowing boundary current, the Benguela Current.

The processes involved in determining the seasonal variability of the BC, the FMC, the BC-FMC confluence zone and the BC separation are of central importance to the regional marine climate. *Olson et al.* [1988] found that a more northward BC separation occurred during the austral winter and spring than during the austral summer and fall. This seasonality may be related to the subtropical high pressure system being centered farther north, with a higher central pressure during the winter and spring [*Peterson and Stramma*, 1991]. This idea, however, was not fully supported by *Olson et al.* [1988]. The mechanisms responsible for this seasonality are still not clear. The seasonal variation of the FMC, the BC, and its separation latitude have been addressed by *Matano et al.* [1993], who used Geosat altimeter data and a barotropic ocean model to argue that both BC and FMC undergo a similar seasonal cycle but with opposite phase. A seasonal signal has also been found in the ACC , with a stronger transport occurring in the austral winter and spring [*Whitworth and Peterson*, 1985]. *Zyryanov and Severov* [1979] presented evidence for a seasonal northward flowing signal in the FMC.

Most attempts to quantitatively describe the circulation of the South Atlantic have been based on an analysis of historical hydrographic data. Examples include the geostrophic calculations by *Gordon and Greengrove* [1986] and *Fu* [1981]. A calculation involving integration along the characteristics of a vorticity equation

[1]Now at College of Oceanic and Atmospheric Sciences, Oregon State University, Corvallis



Paper number 98JC00367.
0148-0227/98/98JC-00367$09.00

(with forcing terms derived from the Levitus data set) was performed by *Mellor et al.* [1982] for the entire South Atlantic. The Fine-Resolution Antarctic Model (FRAM) provides perhaps the most complete robust diagnostic analysis of the South Atlantic [*Webb et al.*, 1991]. However, as with the other studies mentioned above, FRAM does not address the seasonal dependence of the circulation. Using a barotropic model forced by climatological wind stress, *Matano et al.* [1993] showed that the mass transport of the Brazil Current decreases during winter months and increases during summer months. However, they used a limited model domain without the ACC. Further, the results obtained from the barotropic model do not include the effects of density stratification, and the topographic effects may have been amplified. The study by *Matano* [1993], using a three-dimensional model [*Bryan*, 1969] forced by an analytical approximation for the zonally averaged annual mean wind stress, showed the dependence of the Brazil Current separation latitude on the ACC strength at the Drake Passage. A series of experiments also led to the conclusion that if the transport of the FMC is low, the path of the BC is governed by the curl of the wind stress. However, seasonal variation was not discussed in the study.

In this paper the high-resolution primitive equation Princeton Ocean Model [*Blumberg and Mellor*, 1987] is used to study the circulation and seasonal variability in the South Atlantic Ocean. A calculation similar to the "robust-diagnostic" method introduced by *Sarmiento and Bryan* [1982] is first used to simulate the climatological mean field. The model is able to produce a realistic circulation, meridional overturning and heat transport in the South Atlantic Ocean. Next, a prognostic study is carried out. Here the model is forced by the monthly mean wind stress and heat flux. Additionally, a specified seasonal variation in the strength of the ACC is imposed. The results from variation of seasonal circulation suggest that the seasonal variation of ACC plays a dominant role in the season cycle of the BC separation latitute and the strength of the FMC.

The outline of the paper is as follows. In section 2 the ocean model is briefly described, and the implemention of the model and the forcing functions are discussed. The robust diagnostic results are presented in section 3. The results for the seasonal circulation are given in section 4, and the summary and conclusions are presented in section 5.

## 2. Ocean Model

The Princeton Ocean Model is a primitive equation, free surface model. It contains a second moment turbulence closure submodel to provide the vertical mixing coefficients. The model uses the sigma ($\sigma$) coordinate in the vertical direction. The Arakawa-C staggered grid has been adopted in the horizontal directions. Complete thermodynamics have been implemented. Further details of the model are described by *Blumberg and Mellor* [1987]. The model has been extensively used for the

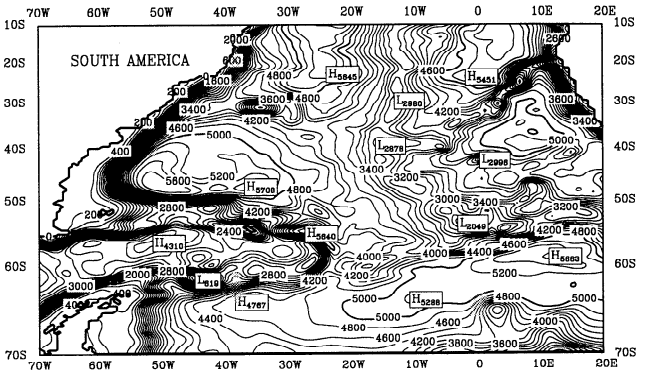


**Figure 1.** Bathymetry of the South Atlantic Ocean.

study of the circulation in various coastal regions. Recently, it has also been used in a basin-scale circulation investigation [*Ezer and Mellor*, 1994].

The model horizontal grid is set with meridians spaced by $\Delta\lambda$=0.5° in east-west direction and $\Delta\lambda$ cos (latitude) in north-south direction. This results in a conformal mapping (Mercator projection). It produces 179 x 179 square grid cells in the South Atlantic Ocean covering the latitude range 10° to 70°S. The mesh size varies from 19 km in the south of the domain to 54 km in the north and is able to resolve the BC, FMC, and associated oceanic eddy field at the mid and high latitudes. The vertical grid uses 11 sigma levels. Topography (Figure 1) is interpolated from the ETOPO5 data (National Geodetic Center, Boulder, Colorado) and has been slightly smoothed in the areas of steep topography to reduce truncation errors [*Haney*, 1991]. To reduce the pressure gradient error in the sigma coordinate formulation [*(Mellor et al.*, 1994], the density gradient is first evaluated on the z level grid $\partial b^*/\partial x^*$ and the sigma grid $\partial b/\partial x$-$(\sigma/H)(\partial b/\partial\sigma)(\partial H/\partial x)$, respectively. Their difference $\varepsilon$ is then determined from

$$\partial b^*/\partial x^* = \partial b/\partial x - (\sigma/H)(\partial b/\partial\sigma)(\partial H/\partial x) + \varepsilon(x,y,\sigma) \quad (1)$$

During all subsequent calculations on the $\sigma$ grid, $\varepsilon$ is used as a correction term and held constant. A similar procedure also applies in the $y$ direction.

The initial potential temperature ($T$) and salinity ($S$) are obtained from *Levitus* [1982] annual climatology data and interpolated onto the model grid. The annual climatology and monthly mean wind stresses of *Hellerman and Rosenstein* [1983] are applied in the diagnostic and prognostic (seasonal variation) studies, respectively. The net surface heat flux into the ocean is calculated in the manner similar to *Gan et al.* [1995, 1996], namely,

$$Q_1 = Q_o - L_a - H_a - LE_a \quad (2)$$

where $Q_o$ is the measured incoming short wave radiation at the surface, $L$ is the latent heat of vaporization ( 2.5 X $10^6$ J $kg^{-1}$ ). $L_a$ is outgoing long wave radiation [*Budyko* 1974], which is given by

$$L_a = \epsilon\sigma T_1^4(0.39 - 0.05e_a^{1/2}(1 - 0.71C^2)) + 4\epsilon\sigma T_a^3(T_1 - T_a) \quad (3)$$

where $\epsilon$ is the emissivity of the ocean (0.97), $\sigma$ is the Stefan-Boltzmann constant, $T_1$ is the sea surface temperature, $e_a$(millibar) is the atmospheric vapor pressure, which can be defined as $e_a = re_{sat}(T_a)$, in which $r$ is the relative humidity and $T_a$ is air temperature, and $C$ is the cloud amount (0-1.0). The sensible and latent heat are calculated by the standard bulk turbulent formula, namely,

$$H_a = \rho_a C_{p,air} C_a \mid W \mid (T_1 - T_a) \quad (4)$$

$$E_a = \rho_a C_L \mid W \mid (e_{sat}(T_1) - re_{sat}(T_a))(\frac{0.622}{p_a}) \quad (5)$$

where $\rho_a$ is air density (1.3 kgm$^{-3}$), $C_{p,air}$=1004 J kg$^{-1}$ K$^{-1}$ is the specific heat of air, $C_a$ (=$10^{-3}$) and $C_L$ (=$10^{-3}$) are the turbulent exchange coefficients, $p_a$ is the sea level pressure, $|W|$ is the wind magnitude, and $e_{sat}$ is the saturation vapor pressure which is computed by the empirical formula given by *Bolton* [1980]

$$e_{sat}(T) = 6.112e^{\frac{17.67T}{T+243.5}} \quad (6)$$

The monthly mean values for $Q_o$, $C$, $T_a$, and $r$ are interpolated from coarse resolution (5° x 5°) data of *Esbensen and Kushnir* [1981]. The surface salinity flux is neglected in the study. In Drake Passage and south of Africa, the barotropic velocities are set to equal to specified transports of the ACC and the (unseparated) Agulhas Current. The flux at Drake Passage is based on the current measurement by *Whitworth and Peterson* [1985], and the strength of Agulhas Current is based on the value given by *Gordon* [1985]. An additional barotropic eastward velocity is then added further south of the African continent, so that the net flux into the model domain vanishes. The resulting velocity profiles are shown in Figure 2. The total transport perpendicular to the northern open boundary is set to zero. Baroclinic components of the velocity on all open boundaries are governed by an Orlanski-type radiation condition.

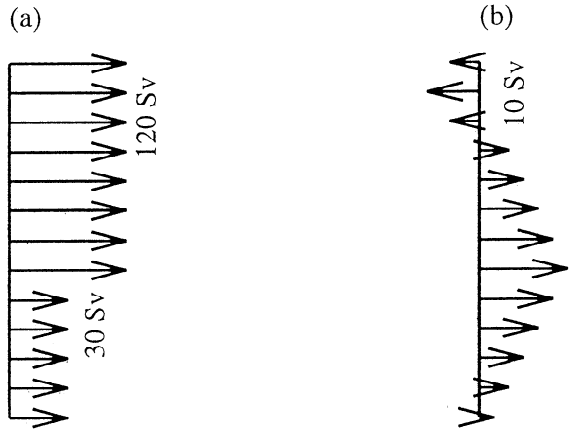


**Figure 2.** Barotropic velocity profiles imposed at (a) the Drake Passage and (b) the eastern boundary.

## 3. Diagnostic Study

In order to obtain the steady wind and density driven circulation based on the observed hydrographic data, a diagnostic run is first performed. That is, holding the temperature and salinity fields fixed, the model equations are time-stepped until a statistical steady state is reached. Comparison of the circulation patterns obtained in this manner with those of previous studies serves as a form of model verification. It also provides a climatological mean state, about which the seasonal variability will be studied in the following section. A similar diagnostic calculation has recently been carried out by *Ezer and Mellor* [1994] for the North Atlantic Ocean. To minimize the errors induced from small-scale density features unresolved by the model, the density should be allowed to deviate from the input field to a certain extent. This can be accomplished by either using a robust-diagnostic method *Sarmiento and Bryan*, 1982] or by conducting a short prognostic calculation following the diagnostic run [*Ezer and Mellor*, 1994]. The robust-diagnostic method is adopted here. It involves the addition of relaxation correction terms in the temperature and salinity equations, which take the form

$$\frac{\partial TD}{\partial t} + \frac{\partial TUD}{\partial x} + \frac{\partial TVD}{\partial y} + \frac{\partial T\omega}{\partial \sigma} = \frac{\partial}{\partial \sigma}(\frac{K_H}{D}\frac{\partial T}{\partial \sigma}) + F_T + \gamma D(T^* - T) \quad (7)$$

$$\frac{\partial SD}{\partial t} + \frac{\partial SUD}{\partial x} + \frac{\partial SVD}{\partial y} + \frac{\partial S\omega}{\partial \sigma} = \frac{\partial}{\partial \sigma}(\frac{K_H}{D}\frac{\partial S}{\partial \sigma}) + F_S + \gamma D(S^* - S) \quad (8)$$

where $D$=$H$+$\eta$ (H=bottom topography and $\eta$=surface elevation), $U$ and $V$ are the eastward and northward velocity components, $\omega$ is the vertical velocity in the $\sigma$ coordinates, $F_T$ and $F_S$ are the horizontal diffusions for the temperature and salinity, respectively, $\gamma$ is an inverse time constant, and $T^*$ and $S^*$ are input fields obtained from observed hydrography data. The parameter $\gamma$ in this study takes the following values:

$$Top\ seven\ \sigma\ surfaces\ \gamma = 1/5\ days \quad (9)$$

$$Deeper\ \sigma\ surfaces\ \gamma = 1/200\ days \quad (10)$$

Thus, the temperature and salinity fields are allowed to deviate substantially from the observed values in the deep ocean but are pegged closely to the climatological values in the upper ocean (approximately top 1000 m). It should be noted that *Sarmiento and Bryan* [1982] used constant $\gamma$ at fixed depth levels. By using large $\gamma$ at the upper $\sigma$ levels, the strong restoring force also applies to the shallow water near the coast where the density may drift quickly away from the climatologi-

cal values. With very large $\gamma$, the model essentially reduces to the diagnostic model. Our results indicate that the circulation is much noisier when a pure diagnostic method is used. On the other hand, applying a small $\gamma$ in the upper part of the ocean results in an unrealistic meridional circulation, particularly in the tropical region.

### 3.1. Surface Elevation and Circulation

The mean fields from the diagnostic calculation provide a useful knowledge for the circulation in the South Atlantic Ocean. Figure 3 shows the model output for the surface elevation and vertically integrated mass transport stream function. Part of the ACC flowing through Drake Passage turns sharply northward east of Drake Passage, flows along the shelf and forms the FMC. This meets with the southward flowing BC at around 43°S, where both currents separate from the coast. The volume transport of the FMC decreases as it flows northward, from 40 Sv at 50°S to 20 Sv at 44°S. Both *Gordon and Greengrove* [1986] and *Piola and Bianchi* [1990] found values of 10 Sv for the FMC at 42°S, whereas, *Peterson* [1990] reports a value of 70 Sv at the same latitude.

The model transport in the BC increases from 10 Sv at 20°S to 30 Sv at 30°S, and then to about 50 Sv near the separation latitude 43°S. *Gordon and Greengrove* [1986] estimated the BC transport to be 19-22 Sv at 38°S. *McCartney and Zemba* [1988], on the other hand, took account of the deep current and arrived at a value of 76 Sv for the total southward geostrophic transport across 37°S. *Mellor et al.* [1982], using a diagnostic model, and *Matano* [1993], using a three-dimentional model [*Bryan*, 1969] obtained values close to 60 Sv. An even larger value, near 75 Sv, was obtained by *Semtner and Chervin* [1992].

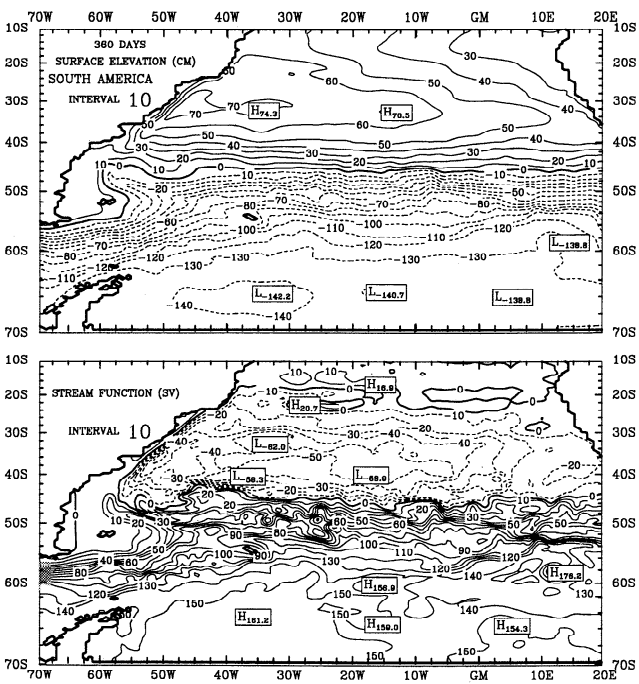


**Figure 3.** (top) Surface elevation and (bottom ) vertically integrated total stream function after 360 days.

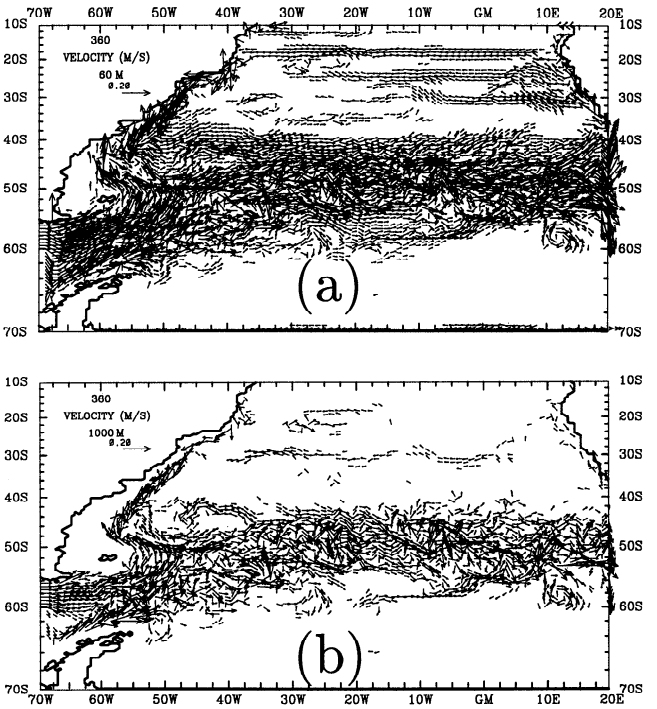


**Figure 4.** Velocity at the depth of (a) 60 m and (b) 1000 m after 360 days. The current speed is truncated at 0.2 m $s^{-1}$

The BC separation latitude of about 43°S seen in our results (Figure 3) is south of the observed separation latitude [*Olson el al.*, 1988]. Further, simple Sverdrup circulation theory implies that the BC should separate along a line where wind curl stress is zero. It seems that the separation latitude of the BC is not dominated by the zero wind stress curl latitude, which is located near 40°S, according to *Hellerman and Rosenstein* [1983] wind data. Many additional factors may influence the location at which separation occurs [*Peterson and Stramma*, 1991], and the relative importance of these remains unclear. In fact, our experiment shows that increasing the strength of the ACC at the Drake Passage will result in the northward movement of the separation latitude. The topic of the BC separation will be discussed in the following sections. After separation, the BC joins with the southward retroflected FMC and continues to flow southward for some distance, while small portions of the FMC continue north along the inner portions of the shelf as shown by the stream function in Figure 3. The seaward extension of the BC that does not recirculate forms the South Atlantic Current (SAC), north of the ACC. The SAC provides the main source for the eastern boundary current of the South Atlantic subtropical gyre, the Benguela Current which bends toward the northwest to separate from the African coast around 30°S (Figure 3).

The sea surface elevation, which indicates the circulation near the surface, varies in response to the ACC and the westerlies from -1.3 m near 60°S to about 0.7

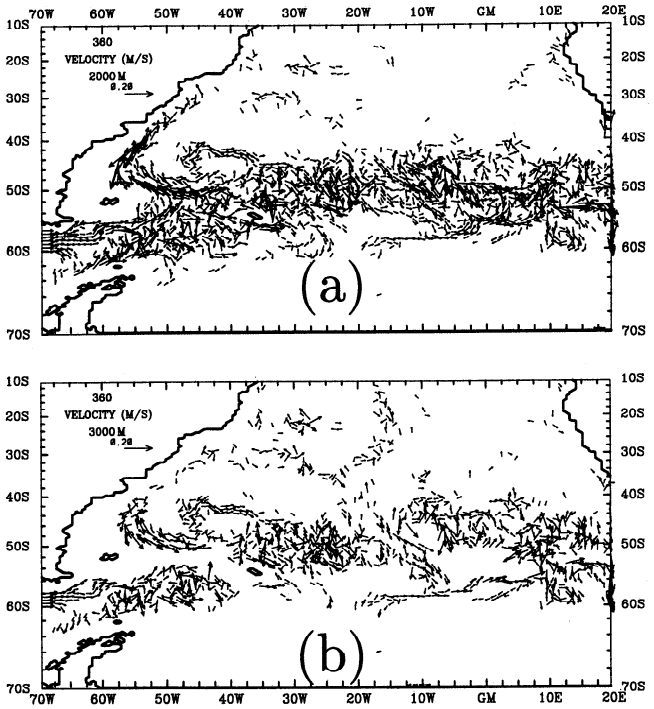


**Figure 5.** Velocity at the depth of (a) 2000 m and (b) 3000 m after 360 days. The current speed is truncated at 0.2 m $s^{-1}$.

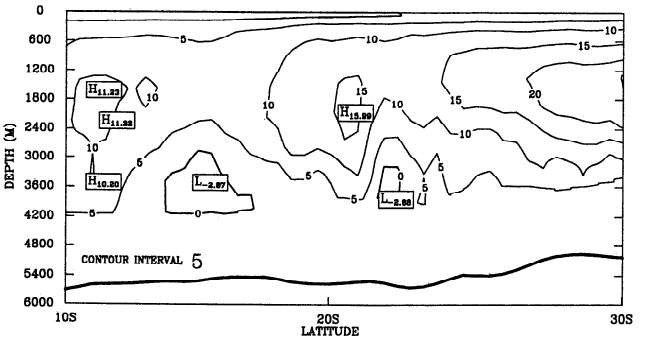


**Figure 6.** Zonally averaged meridional volume transport (Sv) as function of latitude after 360 days.

m at the center of the subtropical gyre (Figure 3). The horizontal velocity field at 60, 1000, 2000 and 3000 m are presented in Figures 4 and 5. Similar to results from *Webb et al.* [1991], the ACC is generally eastward throughout the water column, indicating a strong barotropic component. The confluence zone extends from the surface to about 2000 m. Below 2000 m, a very weak FMC moves northward along the shelf break. Its main stream appears to turn eastward from the confluence zone into the center Argentine Basin. Figure 4 also shows an anticyclonic circulation located east of Rio Grand Rise (near 30°S, 30°W). A similar feature was also found by *Fujio et al.* [1992] who ascribed this feature to potential vorticity conservation of the northward shifting ACC. Near the center of the South Atlantic, a southward flow of deep water occurs near the Mid-Atlantic Ridge, with strong currents near the bottom (Figure 5b). This is similar to the findings of *Saunders and Thompson* [1993] who presented FRAM output. To the east, a strong upper-ocean north-westward Benguela Current occurs just west of the Africa coast near 30°S (Figure 4a). This flow is rather weak at depth, however, and reverses direction below 1000 m. *Reid* [1989] showed a southward geostrophic flow along the southern coast of the eastern boundary above 1500 dbar.

### 3.2. Meridional Mass and Heat Transports

The meridional mass and heat transports are important for maintaining the thermohaline circulation in the Atlantic Ocean. Figure 6 shows the zonally averaged meridional stream function north of Cape of Good Hope. Its structure, with northward/southward volume transport above/below 1200 m is consistent with the results from eddy-resolving global circulation models [*Semtner and Chervin*, 1992; *Fujio et al.*, 1992]. Our model results, however, have less structure near the surface, which may be due to the coarser vertical resolution adopted in the model. The flow from the South Atlantic into the North Atlantic near the surface is about 5 Sv. The equatorward mass transport is mainly carried by the flow at the surface and intermediated waters and is balanced by the southward flow of deep water. *Rintoul* [1991] who used hydrographic data and an inverse method, found that the net transport across a section at at 32°S are 8, 5, and -17 (southward) and 4 Sv for surface, intermediate, deep and bottom waters, respectively. The magnitude of the transport at each layer from our model (Figure 6) is close to the above values.

The characteristics of the meridional heat transport in the South Atlantic are quite different from those in the other oceans of the southern hemisphere. Total heat transport is equatorward north of 33°S, as required by the conveyor belt paradigm [*Hastenrath*, 1980]. The model results are consistent with this feature (Figure 7). The zonal mean meridional overturning is strong between 20°S and 30°S. The upper layers move warm water northward, while the deeper layers advect cold deep water southward. The strongest northward heat transport is about 0.9 PW (1 PW=$10^{15}$ W) near 20°S, even

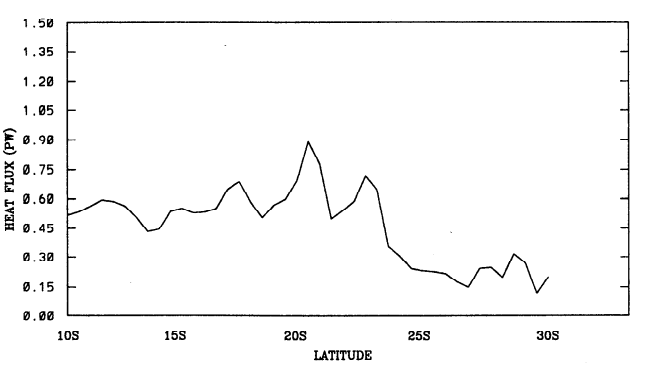


**Figure 7.** Zonally averaged meridional heat transport as function of latitude after 360 days.

though stronger meridional circulation occurs at higher latitudes as shown in Figure 6. This is because of the greater temperature contrast between the surface and deep water there. The transport decreases to smaller values near 30°S (Figure 7). The amplitude and phase of meridional heat flux in Figure 7 are very similar to findings of *Sarmiento* [1986] that showed the strongest heat transport to occur at about 25°S, followed by a sharp decrease at higher latitudes. Also, the meridional flux of heat at 32° is very close to the value of about 0.23 PW from *Rintoul* [1991]. *Fu* [1981], however, found the heat transport to increase from 0.35 PW at 10°S to a maximum of 0.7 PW at 15°S. Southward of this, the heat transport decrease to 0.5 PW near 30°S. Although the meridional heat transport magnitudes and phase vary among the different computational results, their values are all less than 1.0 PW.

As found by *Sarmiento and Bryan* [1982], the vertically integrated meridional mass transport is sensitive to the value of $\gamma$. Our results show that with a uniform and small $\gamma$ all over the domain, a negative cell with poleward current in the upper ocean tends to develop over the entire water column near the tropical region. The reason for this appears to be related to a strong compensation flow at deep levels. The southward/northward currents at the western boundary in this case are stronger in the upper/deeper part of the ocean. However, if a large $\gamma$ is used at the intermediate and upper part of the ocean, the meridional volume transport (Figure 6) is quite similar to the one obtained in the pure diagnostic calculation (Figure 8), although the latter case has a much noisier pattern. It is found that as long as the density near the upper ocean is strongly restored, the model results are not so sensitive to the value of $\gamma$. The difference in the meridional heat flux between the robust and pure diagnostic run is relatively small (Figures 7 and 9).

## 4. Seasonal Variability

Unlike in the diagnostic study above, the density field is now allowed to vary in response to the change of seasonal surface heat flux and horizontal advection of the water. At the open boundaries, when the flow is into the model domain, the prescribed climatological

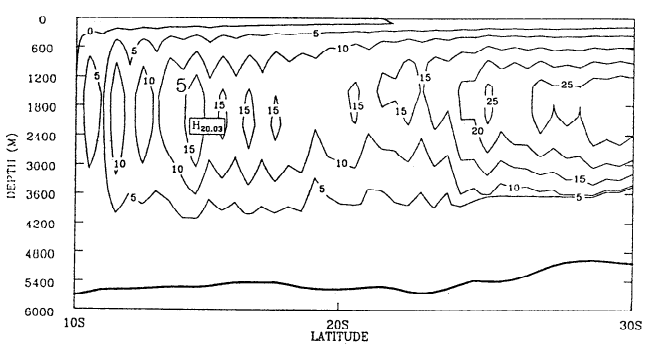


**Figure 8.** Zonally averaged meridional volume transport after 240 days of a pure diagnostic run.

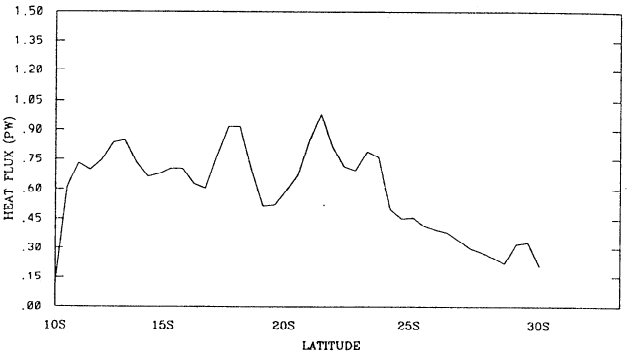


**Figure 9.** Zonally averaged meridional heat transport after 240 days of a pure diagnostic run.

seasonal temperature and salinity are advected into the model domain. In the calculations in sections 4.1 the ACC at the Drake Passage is kept constant (150 Sv) with a velocity profile as shown in Figure 2a. Then in section 4.2 a seasonal variation of the ACC will be imposed to study its effects on the circulation in the South Atlantic Ocean.

To allow the thermal field to reach a steady seasonal cycle, the model is first run for 6 years with monthly mean forcing. The results discussed below are obtained from the output during the seventh year. *Matano* [1993], using a model with similar grid resolution and steady forcing, showed that the model can reach statistical steady state after 3 years of integration. From the FRAM calculations, *Saunders and Thompson* [1993] found that the model reaches quasi-steady state in about 5-6 years. With the seasonal forcing, the steady state in our model is determined by comparing the time series of monthly domain-averaged temperature difference between successive years. This difference between the fifth and sixth year was undetectable.

The objective of this section is to simulate the seasonal variations of both the dynamic and thermodynamic aspects of the South Atlantic circulation. In particular, the variation of the FMC, BC, and its separation characteristics will be discussed.

### 4.1. Variation of Seasonal Circulation and Thermal Field

Figures 10-13 show the modeled seasonal variation of the surface elevation and barotropic circulation in the South Atlantic Ocean due to seasonally varying surface forcing only. In austral summer (defined here as the average over January, February, and March) the surface elevation near the coast of South America (see Figure 1) is slightly higher than in the other seasons. The main surface gyre then weakens after the summer, with the surface elevation being lowest in winter and spring. The seasonal pattern of surface elevation is very similar to the the Geosat altimeter data from *Matano et al.* [1993]. Conditions similar to the sea surface elevation also occur in the depth integrated circulation. The transport for the BC at 40°S is about 50 Sv. The seasonal signal is weak at this latitude. However, to the north, the

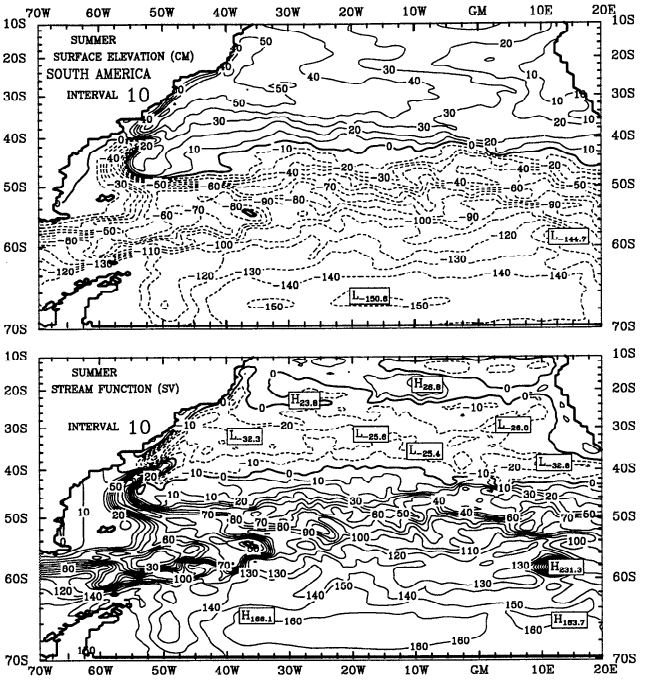


**Figure 10.** (top) Summer mean (January-February-March average) surface elevation and (bottom) vertically integrated total stream function.

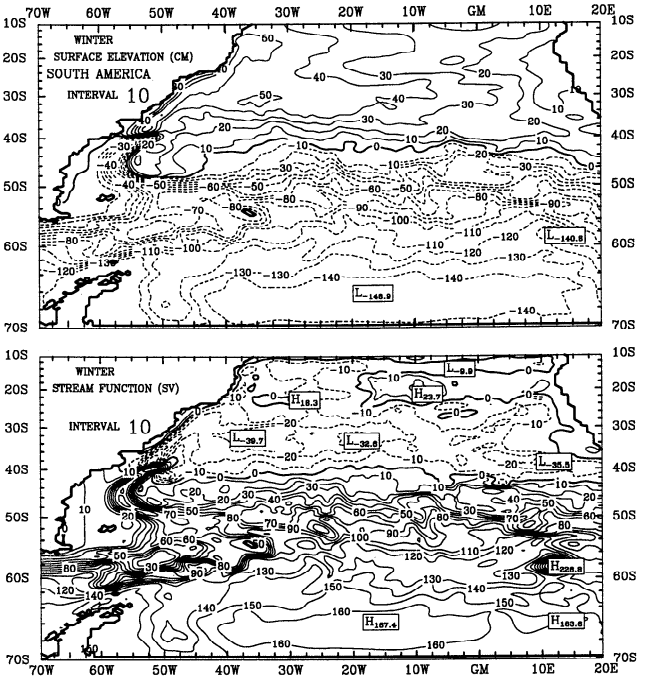


**Figure 12.** (top) Winter mean (July-August-September average) surface elevation and (bottom) vertically integrated total stream function.

BC has a larger seasonal variation. The stronger seasonal BC variation at 40°S obtained by *Matano et al.* [1993] with a wind-driven barotropic model may be due to the lack of the density stratification in their model. The FMC transport slightly increases from summer to fall and winter, and then drops to its smallest value in spring. In response to this variation, the FMC is able to penetrate further north in winter and spring. The phase of the change is consistent with the findings by *Matano et al.* [1993] and *Olson et al.* [1988] who used satellite data to show that the FMC is stronger in winter. Consequently, the separation latitude of the BC moves

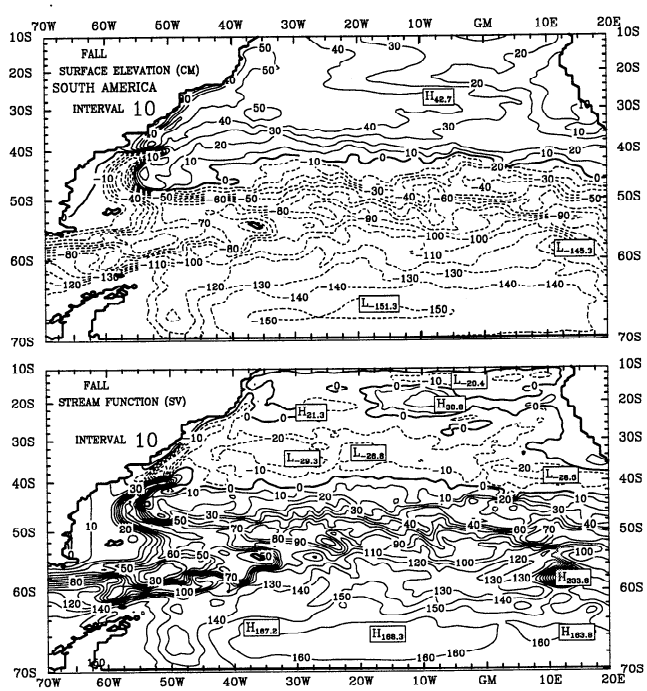


**Figure 11.** (top) Fall mean (April-May-June average) surface elevation and (bottom ) vertically integrated total stream function.

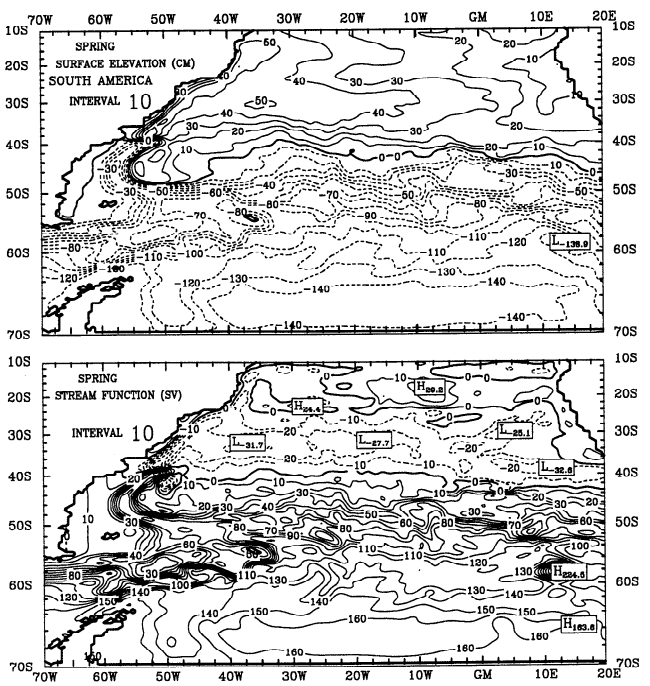


**Figure 13.** (top) Spring mean (October-November-December average) surface elevation and (bottom) vertically integrated total stream function.

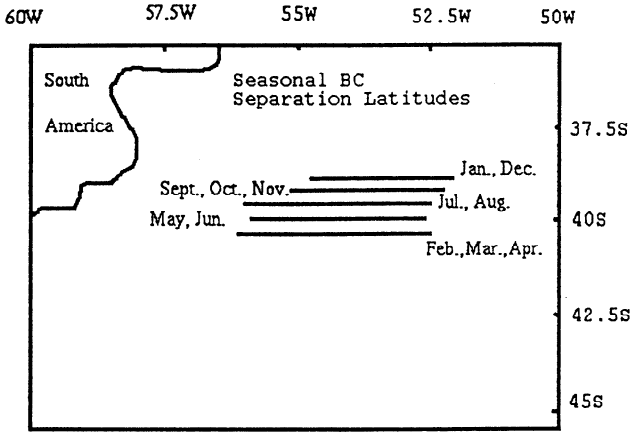


**Figure 14.** Seasonal variation of the BC separation latitude for the case of a stea dy ACC mass transport with the latitudinal profile shown in Figure 2. The contours in the figure are the contours of zero surface elevation from about 200 m depth contour to about 50°W.

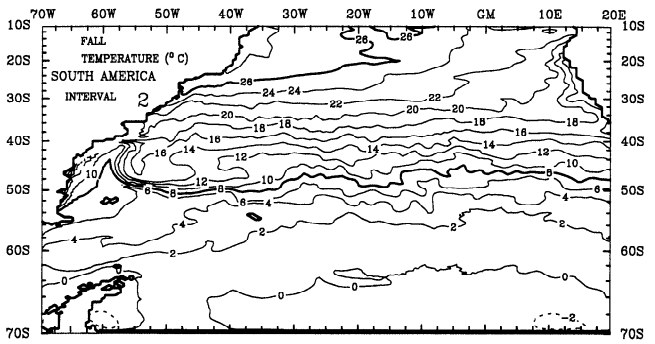


**Figure 16.** Fall mean temperature at the surface.

further north during the winter and spring (Figure 14). The amplitude of this seasonal variation is only about 1° of latitude, which is less than the values estimated from observed data. On the other hand, the climatological data set of *Hellerman and Rosenstein* [1983] indicates that the zero wind stress curl line reaches the northernmost position in winter. However, the very weak seasonal signal from the model results suggest that the wind stress curl may not play a dominant role in controlling the position of the BC separation. In section 4.2 it will be shown that the latitudinal range of the position of the BC separation is significantly enhanced when we allow for temporal dependence in the strength of the ACC flowing through Drake Passage.

The seasonal mean surface temperatures from the model (Figures 15-18) agree well with observed climatological surface temperatures (Figure 19). In summer (Figure. 19a) the tropical warm water (>26°C) extends eastward from Brazil and reaches 20°W. This warm tongue retreats westward in the cold season (Figure 19b). The northward advection of the cold water near the southern coast of Argentina varies with the seasonality of the FMC. As can be seen from the 8°C contour in Figures 15 and 18, the cold water moves northward from about 55°S in summer, to approximately 40°S in winter and then moves southward again in spring. This variation is in phase with the seasonal location of the FMC-BC confluence zone, as indicated in Figure 14. The seasonal sea surface temperature (SST) variation also occurs at higher latitudes. In contrast, temperature variation at depth of 1000 m is very weak (not shown). In comparison with the observations (Figure 19), the model, which has a relatively high resolution, produces many more detailed thermal structures. For example, near the western boundary, the southward invasion of the warm water due to the BC is missed in the Levitus data. The subantarctic front, which forms from the confluence of cold subantarctic water from the FMC and the warm subtropical water from the BC is also not present in the Levitus data. At the eastern boundary, the local wind stress creates an upwelling zone along the Africa coast in the model. The model therefore is able to show smaller scale processes that are believed to be occurring in the real ocean.

### 4.2. Effects of a Time-Dependent ACC Inflow at Drake Passage

As mentioned above, the notable seasonal variation in the western part of the South Atlantic may be related to temporal variations in the strength of the ACC. *Matano* [1993] showed that the latitude of the confluence region is dependent on the nature of inflow in the Drake Passage. When the major part of the ACC is concentrated at the north, he found that the latitude of the confluence region moves northward. Since a large portion of this flux feeds the FMC, it seems reasonable to expect that

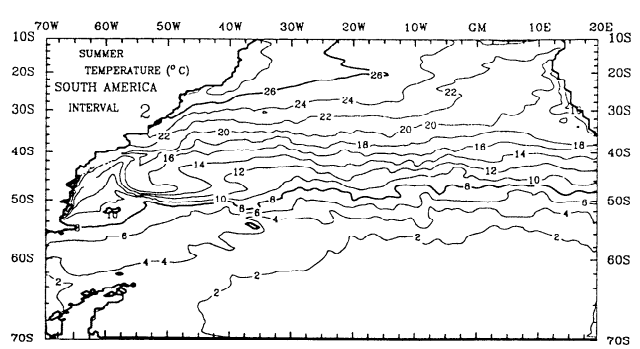


**Figure 15.** Summer mean temperature at the surface.

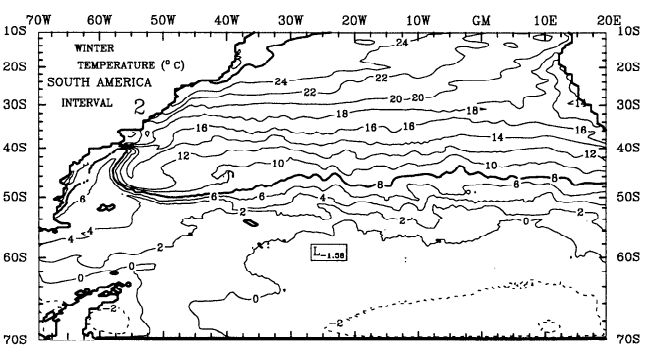


**Figure 17.** Winter mean temperature at the surface.

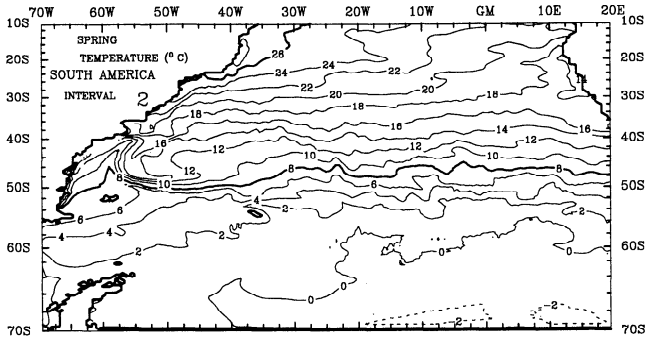


**Figure 18.** Spring mean temperature at the surface.

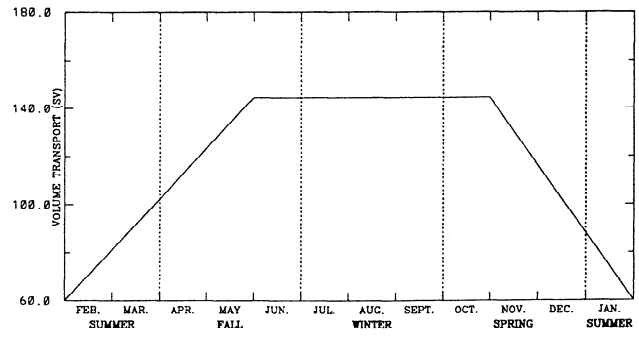


**Figure 20.** Prescribed seasonal ACC mass transport on the northern side of Drake Passage. The annual mean of the total transport at Drake Passage is 150 Sv (see Figure 2).

seasonal variation in the ACC at Drake Passage [*Whitworth and Peterson*, 1995] will drive a similar variation in the FMC, and by extension the position at which the BC separates from the coast. To test this hypotheses, the prescribed seasonal variation in the northern part of the ACC as shown in Figure 20, with phase similar to that estimated for the FMC from Geosat data by *Matano et al.* [1993], is applied to the model. From February through May, the transport increases linearly from 60 to 140 Sv. It is then held constant through to October, after which time it decreases linearly through to the end of January (Figure 20). The annual mean of total transport through the northern part of Drake Passage is kept as 120 Sv.

The results indicate that there is now a much larger variation in the seasonal separation latitude of the BC than in the case with a steady ACC (Figure 21 versus Figure 14). After January the separation latitude of the BC moves southward and reaches the southernmost latitude in April. It then shifts northward and arrives at its northernmost position at the end of the year. It retreats southward in January. On comparing this evolution with the time series of the prescribed ACC amplitude in Figure 20, we note that the southernmost BC separation latitude occurred in April, about 2 months after the minimum ACC volume transport. This time lag is smaller when the transport is larger. The delay is most likely an advective effect since the propagation speed for disturbance traveling northward as an internal Kelvin wave would be of the order 200-300 km $d^{-1}$. It should be noted that the southernmost separation latitude in Geosat data occurs in February [*Matano et al.*, 1993] while our results show that it is in April. This discrepancy is because that, although the ACC transport specified in our model has a phase similar to the FMC strength found by *Matano et al.* [1993], in our model the seasonality is introduced farther away from the confluence zone (i.e. at Drake Passage). This extra distance results in a phase lag in the seasonal migration of the separation latitude. It needs to be pointed out that the southernmost separation latitude based on the Geosat sea level data is at 39°S while our result shows

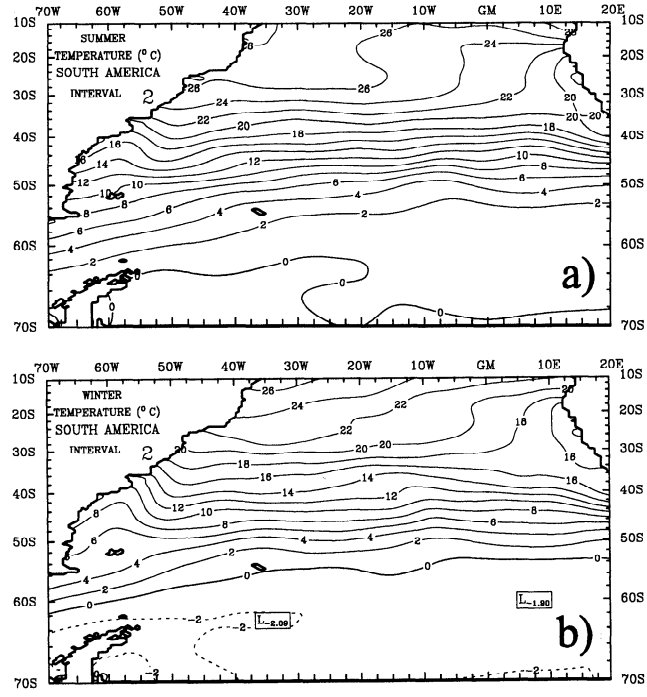


**Figure 19.** Smoothed Levitus's data of SST for (a) summer and (b) winter, mean temperature at the surface.

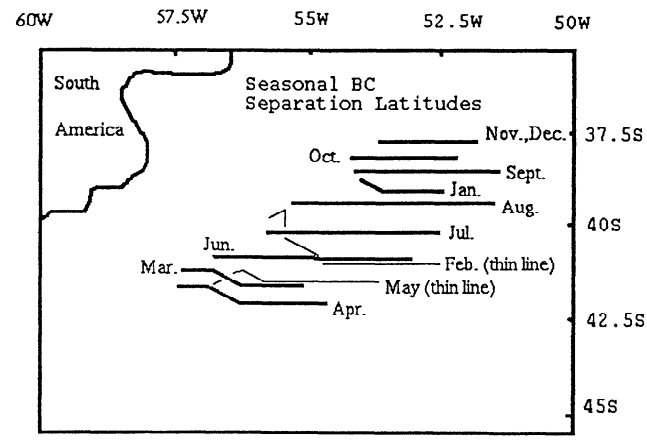


**Figure 21.** Same as Figure 14, but for the case with an unsteady ACC mass transport through the northern part of Drake Passage (see Figure 20).

that it is around 42°S. The difference suggests that the ACC transport imposed may be too small when the separation latitude reaches the southernmost location. The transport of the ACC at Drake Passage varied from the values of 180-120 Sv in previous studies. On the other hand, the latitude of separation obtained from sea level data is sensitive to the method used to define the separation point. The inclusion of the sea level contours instead of one point in results was used to avoid this problem.

For the seasonally varying ACC inflow used, the FMC is stronger in winter ($V_{max}$=0.2 m $s^{-1}$) than in summer ($V_{max}$=0.12 m $s^{-1}$). As compared with the case of steady ACC, the seasonal variation of FMC intensified. It should be realized, however, that there are still not enough observations to claim that the FMC has a seasonal cycle. The connections between the Drake Passage and the northern portion of the Argentinean shelf need to be further investigated. The opposite variation occurs in the simulated BC, which weakens from summer to winter. Additionally, the width of the BC narrows and the strengh of the BC intensifies as it flows south. With a weaker FMC and stronger BC in summer, the FMC-BC confluence zone should be located at a more southerly latitude.

To further establish the dominating effect of a seasonal ACC, we examine the effects of different components of varying atmospheric forcing with a steady ACC. First, we take only a seasonally varying heat flux (Figure 22) and then seasonally varying wind stress (Figure 23). It is found that each of the wind and buoyancy fluxes produces a seasonal signal of the BC separation latitude. With forcing by the seasonally varying heat flux, the separation location moves northward gradually from February and reaches its northernmost latitude at the end of spring. A similar trend occurs in the case with a seasonally varying wind. However, the seasonal signals of the separation latitudinal extent from the seasonally varying wind and buoyancy forcing are weaker than the estimated observed ones. Therefore it is reasonable to suggest that although the seasonal wind and buoyancy variation influence the separation

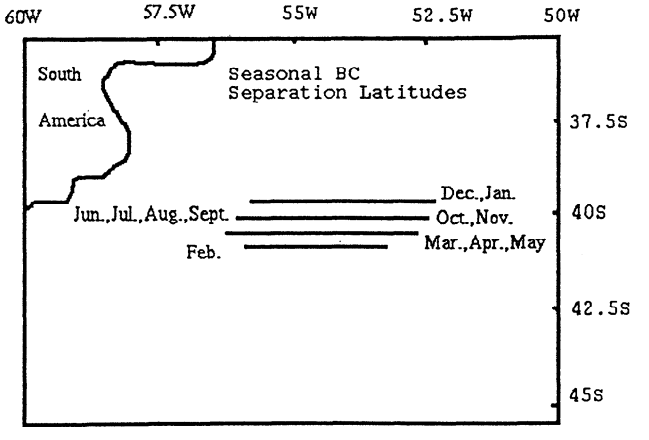


**Figure 22.** Same as Figure 14, but for the case with steady wind stress and steady ACC.

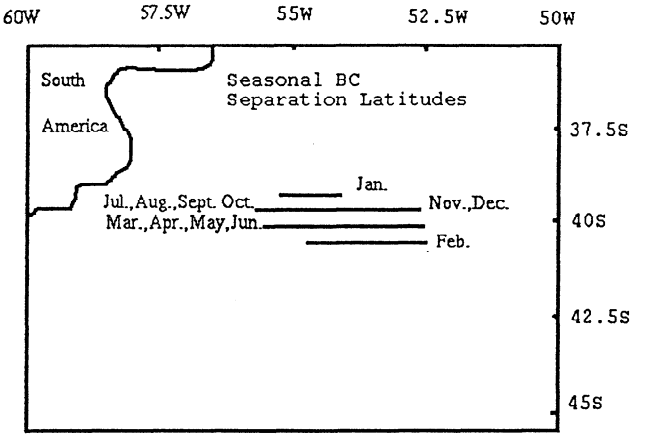


**Figure 23.** Same as Figure 14, but for the case with steady heat flux and steady ACC.

latitude of the BC, the seasonal ACC plays a dominant role on the separation latitude of the BC.

## 5. Summary and Conclusions

The Princeton Ocean Model has been used to simulate the steady and seasonal circulation in the South Atlantic Ocean, in a domain with open boundaries. In the diagnostic calculation, it is found that the model results are much improved by allowing the density field near the bottom to deviate from the input data. The results for the zonally averaged overturning circulation suggest that equatorward transport occurs at the surface and intermediate waters, and poleward flow occurs at the depth. At lower and midlatitudes the zonally averaged meridional heat transport is northward, with a maximum value of nearly 1 PW located near 20°S.

A prognostic simulation for the seasonal variation of the circulation is able to capture the characteristics of the observed variability in the South Atlantic. It is found that the BC has a stronger seasonal variation at the lower latitudes. The inclusion of a seasonal variation in the ACC inflow improves the simulation of the seasonal variations in the confluence region of the BC and the FMC. The results suggest that a seasonally varying ACC plays a dominant role in the BC separation latitude. The effects from a seasonally varying wind stress and heat flux are relatively small. The intensification of the FMC from summer to winter mainly results from the time dependence of the imposed ACC.

While this study has focused on the seasonal cycle of the circulation, it should be noted that there is substantial interannual variability in the South Atlantic and overlying atmosphere [e.g., *Venegas et al.*, 1996; *Olson et al.*, 1988; *Whitworth and Peterson*, 1985]. The inclusion of interannual forcing in the model would further improve our understanding of climate variability in the South Atlantic.

**Acknowledgments.** This research was supported by NSERC and AES grants awarded to L.A.M. and D.N.S and also by a Fonds FCAR Centre grant awarded to the McGill

Centre for Climate and Global Change Research. Computing support from CERCA (Montreal) is also gratefully acknowledged. The authors would like to thank Matano and another reviewer for helpful suggestions.

## References

Blumberg. A. F., and G. L. Mellor, A description of a three-dimensional coastal ocean circulation model, in *Three-Dimensional Coastal Ocean Models, Coastal Estuarine Sci.*, vol. 4, edited by N. S. Heap, pp. 1-16, AGU, Washington, D. C., 1987.

Bolton, D., The computation of equivalent potential temperature, *Mon. Weather Rev., 108*, 1046-1053, 1980.

Bryan, K., A numerical method for the study of the circulation of the world ocean. *J. Comput. Phys., 3*, 347-376, 1969.

Budyko, M. I., *Climate and Life*, 66 pp., Academic, San Diego, Calif., 1974.

Esbensen, S. K., and Y. Kushnir, *OSU Clim. Res. Inst. Rep. 29*, Oreg. State Univ., Corvallis, 1981.

Ezer, T., and G. L. Mellor, Diagnostic and prognostic calculations of the North Atlantic circulation and sea level using a sigma coordinate ocean model, *J. Geophys. Res., 99*, 14,159-14,171, 1994.

Fu, L. L., The general circulation and meridional heat transport of the subtropical South Atlantic determine by inverse methods, *J. Phys. Oceanogr., 11*, 1171-1193, 1981.

Fujio, S., T. Kadowaki, and N. Imasato, World ocean circulation diagnostically derived from hydrographic and wind stress fields, 1, The velocity field, *J. Geophys. Res., 97*, 11,163-11,176, 1992.

Gan, J. P., R. G. Ingram, R. J. Greatbatch and P. Chen, Upper ocean modeling in a coastal bay, *J. Geophys. Res., 100*, 15,977-15,997, 1995.

Gan, J. P., R. G. Ingram, and R. J. Greatbatch, Sensitivity study of upper ocean model in a coastal bay, *J. Mar. Syst., 7*, 203-219, 1996.

Gordon, A. L., Indian-Atlantic transfer of thermocline water at the Agulhas Retroflection, *Science, 227*, 1030-1033, 1985.

Gordon, A. L., and C. Greengrove, Geostrophic circulation of the Brazil-Falkland Confluence, *Deep Sea Res., 33*, 573-585, 1986.

Haney, R. L., On the pressure gradient force over steep topography in sigma-coordinate ocean models, *J. Phys. Oceanogr., 21*, 610-619, 1991.

Hastenrath, S., Heat budget of tropical ocean and atmosphere, *J. Phys. Oceanogr., 10*, 159-170, 1980.

Hellerman, S., and M. Rosenstein, Normal monthly wind stress over the World Ocean with error estimates, *J. Phys. Oceanogr., 13*, 1093-1104, 1983.

Legeckis, R. L., and A. L. Gordon, Satellite observations of the Brazil and Falkland currents: 1975 to 1976, *Deep Sea Res., 29*, 375-401, 1982.

Levitus, S., *Climatological Atlas of the World Ocean*, 173 pp., U.S. Dep. of Commer. and NOAA, Washington, D. C., 1982.

Matano, R. P., On the separation of the Brazil current from the coast, *J. Phys. Oceanogr., 23*, 79-90, 1993.

Matano, R. P., M. G. Schlax, and D. B. Chelton, Seasonal variability in the southwestern Atlantic, *J. Geophys. Res., 98*, 18,027-18,035, 1993.

McCartney, M., and J. Zemba, Thermocline, intermediate and deep circulation in the southwestern South Atlantic (abstract), in *SARRI Meeting Report, May 24-26, pp. 28-29, 1988*, Lamont-Doherty Geol. Obs., Columbia Univ., Palisades, N. Y., 1988.

Mellor, G. L., C. R. Mechoso, and E. Keto, A diagnostic calculation of the general circulation of the Atlantic Ocean, *Deep Sea Res., 29*, 1171-1192, 1982.

Mellor, G. L., T. Ezer, and L. Y. Oey, The pressure gradient conundrum in sigma coordinate ocean models, *J. Atmos. Oceanic Technol., 11*, 1126-1134, 1994.

Olson, D. L., G. P. Podesta, R. H. Evans, and O. Brown, Temporal variations in the separation of Brazil and Malvinas currents, *Deep Sea Res., 35*, 1971-1990, 1988.

Peterson R. G., On the volume transport in the southwestern South Atlantic Ocean (abstract), *Eos Trans. AGU, 71*, 542, 1990.

Peterson, R. G., and L. Stramma, Upper-level circulation in the South Atlantic Ocean. *Prog. Oceanogr., 26*, 1-73, 1991.

Piola, A. R., and A. A. Bianchi, Geostrophic mass transports at the Brazil/Malvinas Confluence (abstract) *Eos Trans. AGU, 71*, 542, 1990.

Reid, J. L., On the total geostrophic circulation of the South Atlantic Ocean: Flow patterns, tracers and transports, *Prog. Oceanogr., 23*, 149-244, 1989.

Reid, J. L., W. D. Nowlin, and W. C. Patzgert, On the characteristics and circulation of the Southwestern Atlantic Ocean, *J. Phys. Oceanogr., 7*, 62-91, 1977.

Rintoul, S. R., South Atlantic interbasin exchange, *J. Geophys. Res., 96*, 2675-2692, 1991.

Sarmiento, J. L., On the north and tropical Atlantic heat balance, *J. Geophys. Res., 91*, 11,677-11,689, 1986.

Sarmiento, J. L., and K. Bryan, An ocean transport model for the North Atlantic, *J. Geophys. Res., 87*, 394-408, 1982.

Saunders, P. M., and S. R. Thompson, Transport, heat, and freshwater fluxed within a diagnostic numerical model (FRAM), *J. Phys. Oceanogr., 23*, 452-464, 1993.

Semtner, A. J., and R. M. Chervin, Ocean general circulation from a global eddy-resolving model, *J. Geophys. Res., 97*, 5493-5550, 1992.

Venegas, S. V., L. A. Mysak, and D. N. Straub, Evidence for interannual and interdecadal climate variability in the South Atlantic, *Geophys. Res. Lett., 23*, 2673-2676, 1996.

Webb, D. J., et al. (The FRAM Group), An eddy-resolving model of the Southern Ocean, *Eos Trans. AGU, 72*, 169, 174-175, 1991.

Whitworth, T., III and R. G. Peterson, Volume transport of the Antarctic Circumpolar Current from bottom pressure measurements, *J. Phys. Oceanogr., 15*, 810-816, 1985.

Zyryanov, V. N., and D. N. Severov, Water circulation in the Falkland-Patagonia region and its seasonal variation, *Oceanology*, Engl. Transl., *19*, 518-522, 1979.

J. P. Gan, College of Oceanic and Atmospheric Sciences, Oregon State University, 104 Ocean Admin Building, Corvallis, OR 97331-5503. (e-mail: gan@oce.orst.edu)

L. A. Mysak and D. N. Straub, Department of Atmospheric and Oceanic Sciences, McGill University, Montreal, Quebec, Canada, H3A 2K6. (e-mail: mysak@zephyr.meteo.mcgill.ca; david@gumbo.meteo.mcgill.ca)

(Received February 19, 1997; revised September 18, 1997; accepted December 10, 1997.)